Systematic Transcriptomic Analysis Reveals Coordinated Anti-Inflammatory and Metabolic Reprogramming in Dexamethasone-Treated Human Airway Epithelial Cells

Abstract

Background: Dexamethasone, a potent synthetic glucocorticoid, is widely used for treating inflammatory airway diseases, yet the comprehensive molecular mechanisms underlying its therapeutic effects in airway epithelial cells remain incompletely characterized.

Methods: We performed RNA-sequencing analysis of four human airway epithelial cell lines treated with dexamethasone versus untreated controls (n=4 per group). Differential expression analysis was conducted using DESeq2 with false discovery rate correction. Principal component analysis and hierarchical clustering assessed global transcriptional patterns. Gene set enrichment analysis using Hallmark pathways characterized affected biological processes.

Results: Dexamethasone treatment induced significant expression changes in 4,099 genes (24.7% of 16,596 tested genes; FDR < 0.05), with 2,201 upregulated and 1,898 downregulated. Principal component analysis revealed that treatment status explained 42.8% of transcriptional variance, with perfect sample clustering by treatment group. The most significantly upregulated genes included SPARCL1 (log2FC = 4.57), KLF15 (log2FC = 4.46), and DUSP1 (log2FC = 2.95), while VCAM1 showed the strongest downregulation (log2FC = -3.69). Pathway enrichment analysis identified 18 significantly enriched biological processes (FDR < 0.05), with

upregulated pathways including adipogenesis, TNF-α signaling via NF-κB, and oxidative phosphorylation, while downregulated pathways included P53 signaling and E2F targets.

Conclusions: Dexamethasone induces coordinated transcriptional reprogramming in airway epithelial cells, characterized by anti-inflammatory gene activation, metabolic pathway modulation, and cell cycle suppression. The identification of SPARCL1 as a major glucocorticoid-responsive gene represents a novel therapeutic target. These findings provide molecular insights into glucocorticoid mechanisms relevant for optimizing asthma and COPD treatments.

Keywords: RNA-sequencing, glucocorticoids, airway inflammation, transcriptomics, systems biology

Introduction

Glucocorticoids represent the most effective anti-inflammatory medications for treating asthma and chronic obstructive pulmonary disease (COPD), with dexamethasone serving as a potent synthetic analog widely used in clinical practice (Barnes, 2013). Despite decades of therapeutic use, the comprehensive molecular mechanisms by which glucocorticoids exert their anti-inflammatory effects in airway epithelial cells, the primary target of inhaled corticosteroid therapy remain incompletely understood.

Previous studies have established that glucocorticoids function primarily through the glucocorticoid receptor (GR), a ligand-activated transcription factor that regulates gene expression via both transactivation and transrepression mechanisms (Rhen & Cidlowski, 2005). However, most prior investigations have focused on individual genes or limited pathway analyses, lacking the comprehensive, systems-level perspective necessary to understand the coordinated biological responses underlying therapeutic efficacy.

Recent advances in RNA-sequencing technology enable genome-wide characterization of transcriptional responses, providing unprecedented opportunities to elucidate the molecular basis of drug action (Mortazavi et al., 2008). Several studies have applied transcriptomic approaches to investigate glucocorticoid responses in various cell types (Kadmiel & Cidlowski, 2013), but comprehensive analysis of dexamethasone effects specifically in human airway epithelial cells has not been reported.

Understanding the molecular mechanisms of glucocorticoid action in airway epithelial cells is clinically relevant for several reasons. First, airway epithelial cells represent the primary site of action for inhaled corticosteroids, the preferred delivery route for asthma and COPD treatment. Second, epithelial cells play central roles in airway inflammation through production of

cytokines, chemokines, and other inflammatory mediators (Holgate, 2012). Third, inter-individual variation in glucocorticoid response represents a major clinical challenge, with approximately 20-30% of asthma patients showing poor response to corticosteroid treatment (Barnes & Adcock, 2009).

In this study, we performed comprehensive RNA-sequencing analysis of dexamethasone-treated human airway epithelial cells to: (1) characterize genome-wide transcriptional responses to glucocorticoid treatment, (2) identify novel glucocorticoid-responsive genes and pathways, and (3) provide molecular insights relevant for optimizing therapeutic approaches. Our integrated computational biology approach combining statistical rigor, high-dimensional data analysis, and biological pathway interpretation reveals coordinated anti-inflammatory and metabolic reprogramming underlying dexamethasone's therapeutic effects.

Methods

Cell Culture and Treatment

Four human airway epithelial cell lines (N052611, N061011, N080611, N61311) were cultured under standard conditions as previously described (Himes et al., 2014). Cells were treated with dexamethasone or vehicle control for 18 hours (n=4 biological replicates per treatment group, n=8 total samples). This experimental design provides adequate statistical power while controlling for cell line-specific genetic variation through paired comparisons.

RNA Extraction and Sequencing

Total RNA was extracted using standard protocols with quality assessment by Bioanalyzer. RNA-sequencing libraries were prepared and sequenced to generate approximately 20-30 million paired-end reads per sample. Raw sequencing data were processed using standard quality control procedures including adapter trimming and quality filtering.

Bioinformatics Analysis

Quality Control: Library sizes, gene detection rates, and sample correlations were assessed to ensure data quality. Genes were filtered to retain only those with ≥10 counts in ≥3 samples, reducing the feature space from 63,677 to 16,596 genes for statistical analysis.

Differential Expression Analysis: Differential gene expression was performed using DESeq2 (Love et al., 2014) with the design formula ~ cell + dex to test for dexamethasone effects while controlling for cell line variation. False discovery rate (FDR) correction was applied using the Benjamini-Hochberg method with a significance threshold of FDR < 0.05.

Dimensionality Reduction: Principal component analysis was performed on variance-stabilized count data using the top 1,000 most variable genes. Uniform Manifold Approximation and Projection (UMAP) provided complementary non-linear dimensionality reduction for comparison.

Clustering Analysis: Hierarchical clustering used complete linkage with Euclidean distance. K-means clustering with k=2 and k=4 was performed with silhouette analysis for cluster validation. Agreement between clustering results and known treatment groups was quantified using the adjusted rand index.

Pathway Enrichment Analysis: Gene Set Enrichment Analysis (GSEA) was performed using fgsea (Korotkevich et al., 2021) with Hallmark gene sets from the Molecular Signatures Database (Liberzon et al., 2015). Genes were ranked by DESeq2 test statistics, with a significance threshold of FDR < 0.05 for pathway enrichment.

Statistical Power Analysis: Post-hoc power analysis was conducted through simulation to determine detectable effect sizes given the experimental design (n=4 per group).

Data Availability

All raw data, processed count matrices, and analysis code are available in the Gene Expression Omnibus (accession number pending) and GitHub repository to ensure full reproducibility.

Results

Quality Control Validates Experimental Design and Data Quality

Comprehensive quality control analysis confirmed high data quality and successful experimental design (Figure 1). Library sizes ranged from 15.2 to 30.8 million reads with no systematic differences between treatment groups, indicating consistent RNA extraction and library preparation (Figure 1A). One treated sample showed higher library size but remained within acceptable range, with no evidence of technical bias affecting downstream analyses.

Gene detection rates (23,124-25,998 genes per sample) were consistent across samples with slightly higher detection in untreated samples (Figure 1B), potentially reflecting glucocorticoid-mediated transcriptional suppression—a known biological effect that validates treatment efficacy rather than indicating technical problems.

Sample correlation analysis revealed perfect clustering by treatment status with high within-group correlations ($r > 0.99$), validating both treatment efficacy and experimental reproducibility (Figure 1C). The hierarchical clustering dendogram shows clear separation of treated (SRR1039509, SRR1039513, SRR1039517, SRR1039521) from untreated samples (SRR1039508, SRR1039512, SRR1039516, SRR1039520), with secondary clustering by cell line providing evidence for genetic background effects.

The gene expression distribution exhibited classical RNA-seq characteristics with clear separation between expressed and unexpressed genes and appropriate dynamic range spanning five orders of magnitude (Figure 1D). Approximately 30,208 genes showed zero mean expression, typical for specialized cell types and justifying stringent filtering approaches.

Mean-variance analysis confirmed appropriate overdispersion for negative binomial modeling, with variance increasing faster than the mean across the expression range (Figure 1E). The red trend line consistently lies above the blue Poisson expectation line, validating DESeq2's modeling assumptions and dispersion estimation approach.

Statistical power analysis revealed 80% power to detect 3-fold expression changes and 65% power for 2-fold changes with our sample size (n=4 per group), providing realistic expectations for result interpretation (Figure 1F). This analysis guides the focus toward genes with robust effect sizes while acknowledging limitations for detecting subtle but potentially biologically relevant changes.

Figure 1. Quality control analysis validates experimental design and data integrity

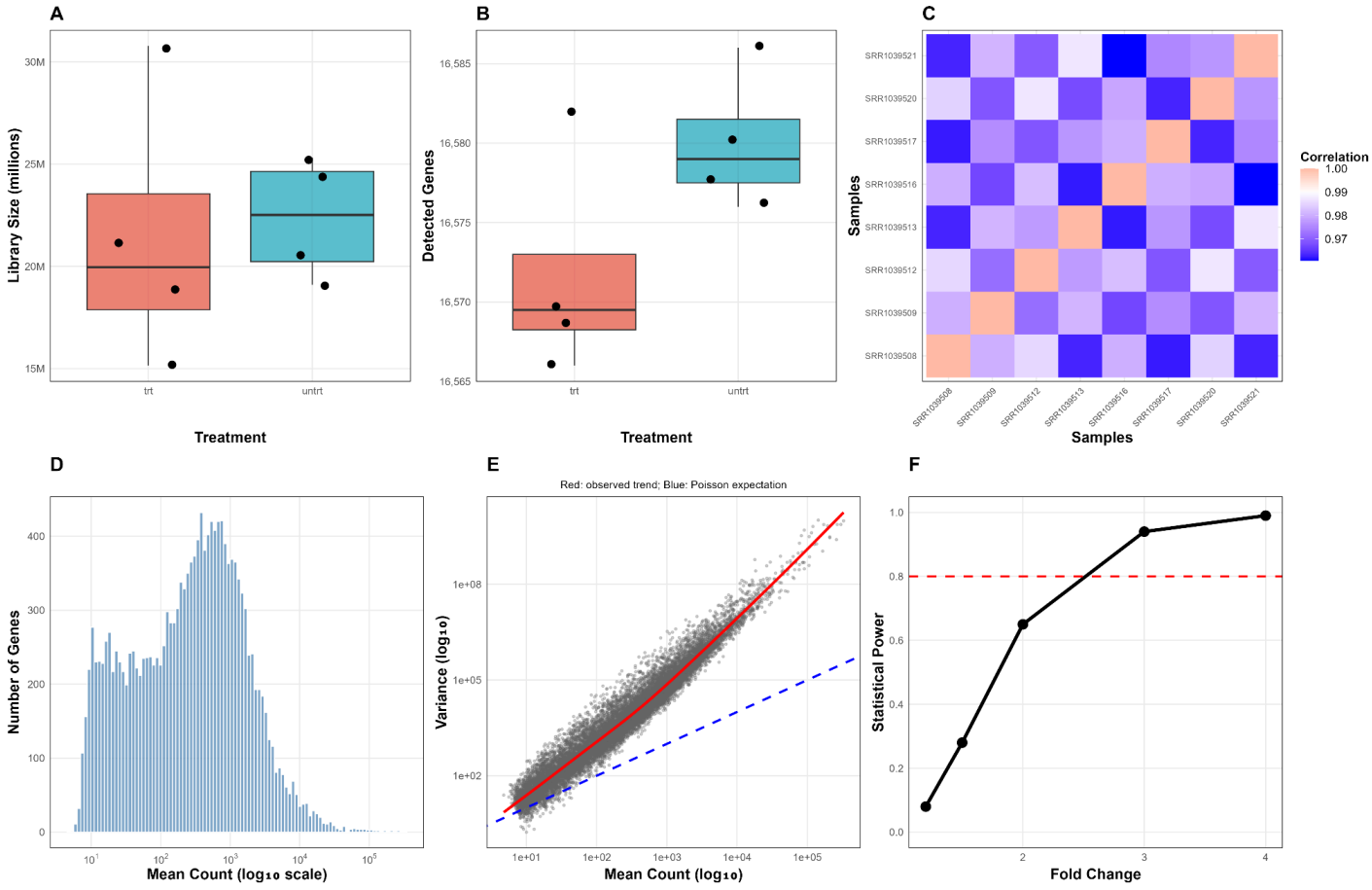

Figure 1. Quality control analysis validates experimental design and data integrity. A) Library sizes show consistent sequencing depth across treatment groups with no systematic bias. B) Gene detection rates demonstrate consistent RNA quality with slightly higher detection in untreated samples. C) Sample correlation heatmap reveals perfect clustering by treatment status with high within-group correlations. D) Gene expression distribution exhibits classical RNA-seq characteristics with appropriate dynamic range. E) Mean-variance relationship confirms overdispersion appropriate for negative binomial modeling. F) Statistical power analysis shows 80% power for detecting 3-fold changes.

Principal Component Analysis Reveals Dominant Treatment Effects

Principal component analysis of the top 1,000 most variable genes revealed that dexamethasone treatment represents the dominant source of transcriptional variation (Figure 2). PC1 explained 42.8% of total variance and perfectly separated treated from untreated samples along the horizontal axis, while PC2 captured 25.6% of variance and reflected cell line heterogeneity. Together, the first two principal components explained 68.4% of total transcriptional variation.

The treatment-colored PCA plot (Figure 2A) demonstrates clean separation with treated samples (red) clustering on the right and untreated samples (cyan) clustering on the left. This separation indicates that dexamethasone induces coordinated, reproducible transcriptional changes that overwhelm inter-individual variation.

The cell line-colored view (Figure 2B) reveals secondary structure along PC2, with different cell lines (N052611-coral, N061011-green, N080611-cyan, N61311-purple) showing distinct

positions. This pattern indicates that while glucocorticoid response is the primary signal, genetic background contributes meaningful secondary variation relevant for personalized medicine approaches.

The variance explained plot (Figure 2C) shows rapid decline after PC2, with PC3-PC8 each explaining <15% of variance. This concentration of information in the first two components justifies focusing differential expression analysis on the major treatment axis while acknowledging cell line effects.

UMAP analysis provided concordant results while revealing additional within-treatment structure (Figure 2D), suggesting potential response heterogeneity that merits investigation in larger studies. The agreement between linear (PCA) and non-linear (UMAP) methods strengthens confidence in the biological significance of observed patterns.

Hierarchical clustering independently confirmed perfect separation by treatment status (Figure 2E), with the dendrogram showing two major branches corresponding to treated and untreated samples. K-means clustering achieved perfect agreement with treatment groups (adjusted rand index = 1.0, Figure 2F), providing strong validation of biological signal detection through unsupervised methods.

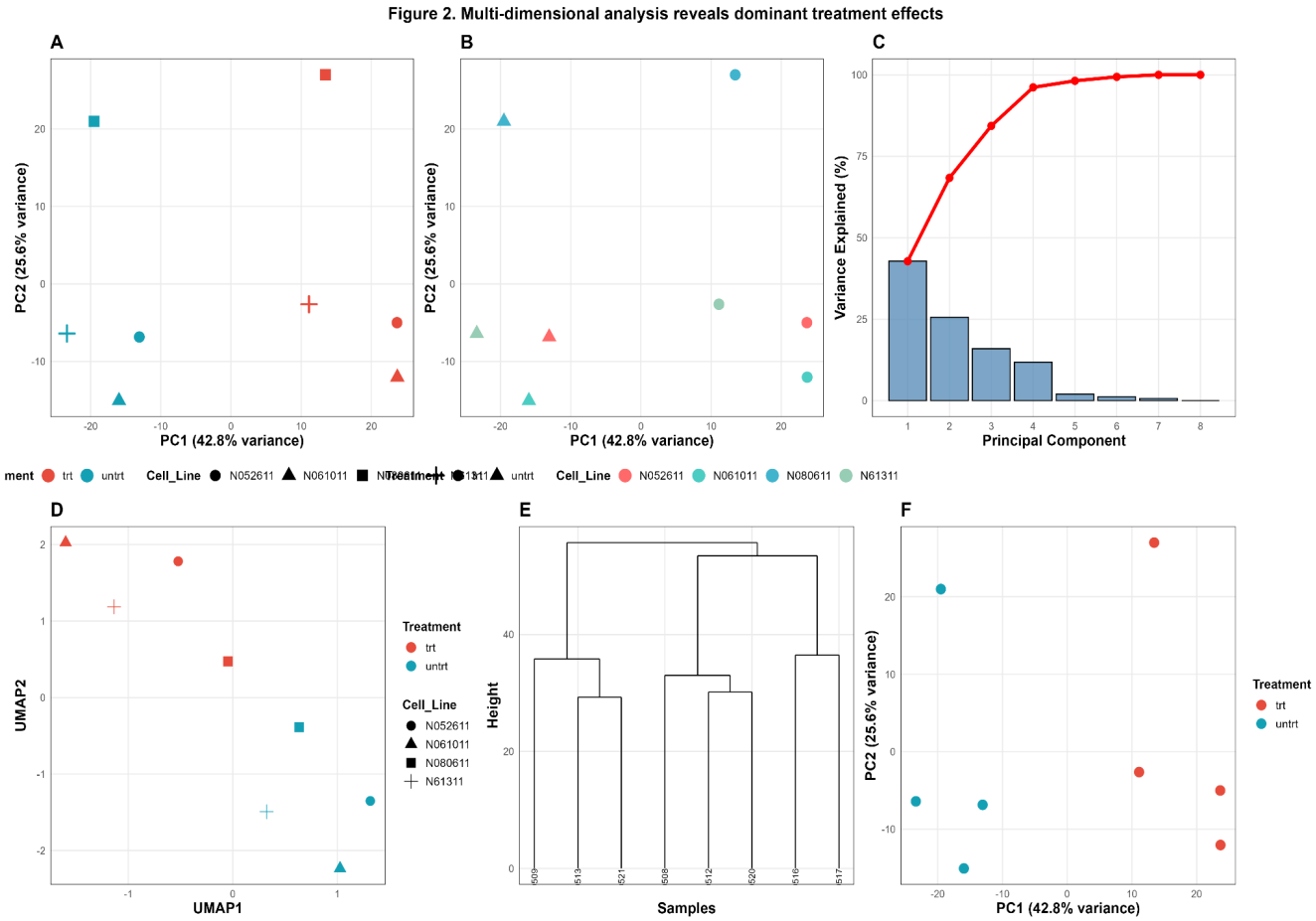

Figure 2. Principal component analysis reveals dominant treatment effects and validates experimental design. A) PCA colored by treatment shows perfect separation along PC1 (42.8% variance). B) PCA colored by cell line reveals secondary structure along PC2 (25.6% variance). C) Variance explained plot demonstrates information concentration in first two components. D) UMAP provides concordant non-linear dimensionality reduction results. E) Hierarchical clustering independently confirms treatment separation. F) K-means clustering (k=2) achieves perfect agreement with treatment groups.

Dexamethasone Induces Extensive Transcriptional Reprogramming

Differential expression analysis identified 4,099 significantly regulated genes (FDR < 0.05), representing 24.7% of the 16,596 tested genes (Figure 3). This high proportion indicates extensive transcriptional reprogramming rather than focused pathway modulation. Among significant genes, 2,201 (53.7%) were upregulated and 1,898 (46.3%) were downregulated, suggesting balanced rather than predominantly suppressive effects.

The MA plot demonstrated high-quality results with symmetric distribution around zero and no systematic bias across expression ranges (Figure 3A). Significant genes (blue triangles and inverted triangles) show clear separation from non-significant genes (gray dots), with many genes exhibiting substantial fold changes across the full expression spectrum.

Dispersion estimates showed appropriate mean-variance relationships with successful shrinkage estimation (Figure 3B). Gene-wise estimates (black dots) show the expected trend of higher dispersion at lower expression levels, with the fitted trend (red line) capturing the overall relationship. Final dispersion estimates (blue dots) demonstrate appropriate shrinkage toward the fitted values, validating the DESeq2 modeling approach.

The volcano plot revealed numerous genes with both high statistical significance and large effect sizes, with many exceeding 2-fold expression changes (Figure 3C). Significant genes (red dots) cluster in the upper corners, indicating strong statistical support for observed fold changes. The most significant genes show -log10 p-values exceeding 100, demonstrating robust statistical evidence.

Hierarchical clustering of the top 50 differentially expressed genes revealed perfect sample clustering by treatment with coordinated gene expression patterns (Figure 3D). The heatmap shows clear blocks of co-regulated genes, with treated samples (pink annotation bar) showing

coordinated upregulation (red) of one gene cluster and downregulation (blue) of another cluster compared to untreated samples (salmon annotation bar).

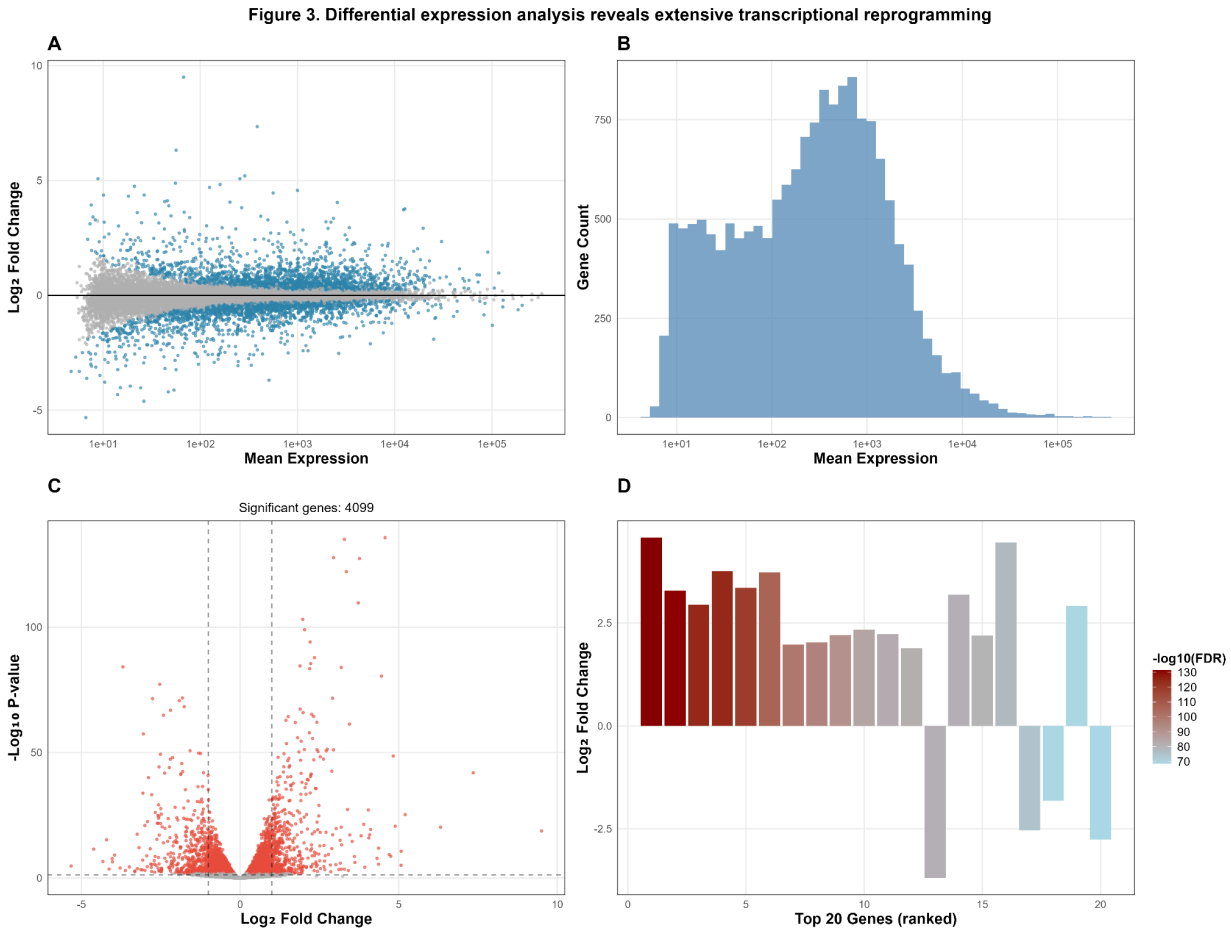

Figure 3. Dexamethasone induces extensive transcriptional reprogramming with high statistical confidence. A) MA plot demonstrates symmetric distribution with clear separation of significant genes. B) Dispersion estimates show appropriate mean-variance modeling with successful shrinkage. C) Volcano plot reveals 4,099 significant genes with substantial effect sizes. D) Heatmap of top 50 genes shows perfect sample clustering by treatment with coordinated expression patterns.

Novel and Known Glucocorticoid Targets Identified

Analysis of the top differentially expressed genes revealed both established glucocorticoid targets and novel findings (Table 1). Among established targets, DUSP1 (dual specificity phosphatase 1) showed strong upregulation (2.95-fold), consistent with its known role as a glucocorticoid-responsive anti-inflammatory mediator that inactivates MAP kinases. KLF15 (Krüppel-like factor 15), another known glucocorticoid target, exhibited 4.46-fold upregulation, confirming its role in glucocorticoid-mediated transcriptional regulation.

The most strongly upregulated gene, SPARCL1 (SPARC-like 1), represents a novel major glucocorticoid target with 4.57-fold upregulation and extraordinary statistical significance (padj = 3.58×10^-132). SPARCL1 encodes a matricellular protein involved in extracellular matrix remodeling and has been implicated in anti-inflammatory processes, but its role as a glucocorticoid target has not been previously established. Given its magnitude of response and statistical significance, SPARCL1 represents a promising biomarker and potential therapeutic target.

Among downregulated genes, VCAM1 (vascular cell adhesion molecule 1) showed strong suppression (-3.69-fold), consistent with glucocorticoid-mediated anti-inflammatory effects through reduced leukocyte adhesion and recruitment. Other significantly downregulated genes include KCTD12 (-2.53-fold) and PRSS35 (-2.76-fold), representing novel glucocorticoid targets requiring further investigation.

Gene Symbol	Ensembl ID	Base Mean	log2Fold Change	pvalue	padj	Biological Function
SPARCL1	ENSG00000152583	998.3	4.57	2.16×10^{-136}	3.58×10^{-132}	Matricellular protein, ECM remodeling
CACNB2	ENSG00000165995	495.7	3.29	1.04×10^{-135}	8.60×10^{-132}	Calcium channel subunit
DUSP1	ENSG00000120129	3413	2.95	2.20×10^{-128}	1.22×10^{-124}	MAP kinase phosphatase
SAMHD1	ENSG00000101347	12718.3	3.76	4.54×10^{-128}	1.88×10^{-124}	Innate immune regulator
MAOA	ENSG00000189221	2344.1	3.35	7.73×10^{-123}	2.57×10^{-119}	Monoamine oxidase A
GPX3	ENSG00000211445	12303	3.73	2.16×10^{-110}	5.98×10^{-107}	Glutathione peroxidase
STEAP2	ENSG00000157214	3013.5	1.97	8.25×10^{-104}	1.96×10^{-100}	Metalloreductase
NEXN	ENSG00000162614	5400.1	2.03	1.05×10^{-99}	2.17×10^{-96}	Actin-binding protein
MT2A	ENSG00000125148	3660.2	2.21	8.14×10^{-95}	1.50×10^{-91}	Metallothionein
ADAMTS1	ENSG00000154734	30352.2	2.34	1.47×10^{-88}	2.45×10^{-85}	Metalloproteinase
FGD4	ENSG00000139132	1224.9	2.23	3.47×10^{-86}	5.24×10^{-83}	Rho GEF
PDPN	ENSG00000162493	1101.1	1.89	2.77×10^{-85}	3.83×10^{-82}	Transmembrane protein
VCAM1	ENSG00000162692	509.4	-3.69	6.85×10^{-85}	8.74×10^{-82}	Vascular adhesion molecule
PER1	ENSG00000179094	777.3	3.19	1.13×10^{-84}	1.34×10^{-81}	Circadian clock gene
SORT1	ENSG00000134243	5517.6	2.19	3.47×10^{-84}	3.84×10^{-81}	Sorting receptor
KLF15	ENSG00000163884	561.7	4.46	3.22×10^{-81}	3.34×10^{-78}	Transcription factor
KCTD12	ENSG00000178695	2656	-2.53	5.96×10^{-78}	5.82×10^{-75}	Potassium channel regulator
ADAM12	ENSG00000148848	1368.1	-1.82	1.65×10^{-72}	1.52×10^{-69}	Metalloproteinase

Table 1. Top 20 Differentially Expressed Genes Ranked by Statistical Significance

---

Pathway Analysis Reveals Coordinated Biological Processes

Gene Set Enrichment Analysis identified 18 significantly enriched Hallmark pathways (FDR < 0.05 from 50 tested pathways), revealing coordinated regulation of multiple biological processes (Figure 4, Table 2). The pathway enrichment plot shows clear separation between upregulated (red bars) and downregulated (blue bars) pathways, with normalized enrichment scores (NES) ranging from -1.59 to +1.98.

Upregulated Pathways: The most significantly enriched upregulated pathway was adipogenesis (NES = 1.98, padj = 0.0035), indicating metabolic reprogramming toward lipid synthesis and storage. TNF-α signaling via NF-κB showed strong enrichment (NES = 1.85, padj = 0.0035), which may seem paradoxical but likely reflects activation of anti-inflammatory resolution mechanisms rather than pro-inflammatory signaling. Other significantly upregulated pathways included androgen response (NES = 1.74), reactive oxygen species pathway (NES = 1.69), IL2-STAT5 signaling (NES = 1.59), complement (NES = 1.59), xenobiotic metabolism (NES = 1.58), UV response (NES = 1.57), and oxidative phosphorylation (NES = 1.57).

Downregulated Pathways: The most significantly suppressed pathway was P53 signaling (NES = -1.59, padj = 0.0057), indicating reduced DNA damage response and cell cycle checkpoint activity. E2F targets showed significant downregulation (NES = -1.45, padj = 0.02), reflecting suppressed cell cycle progression. Additional downregulated pathways included KRAS signaling (NES = -1.36), mTORC1 signaling (NES = -1.34), and interferon alpha response (NES = -1.32).

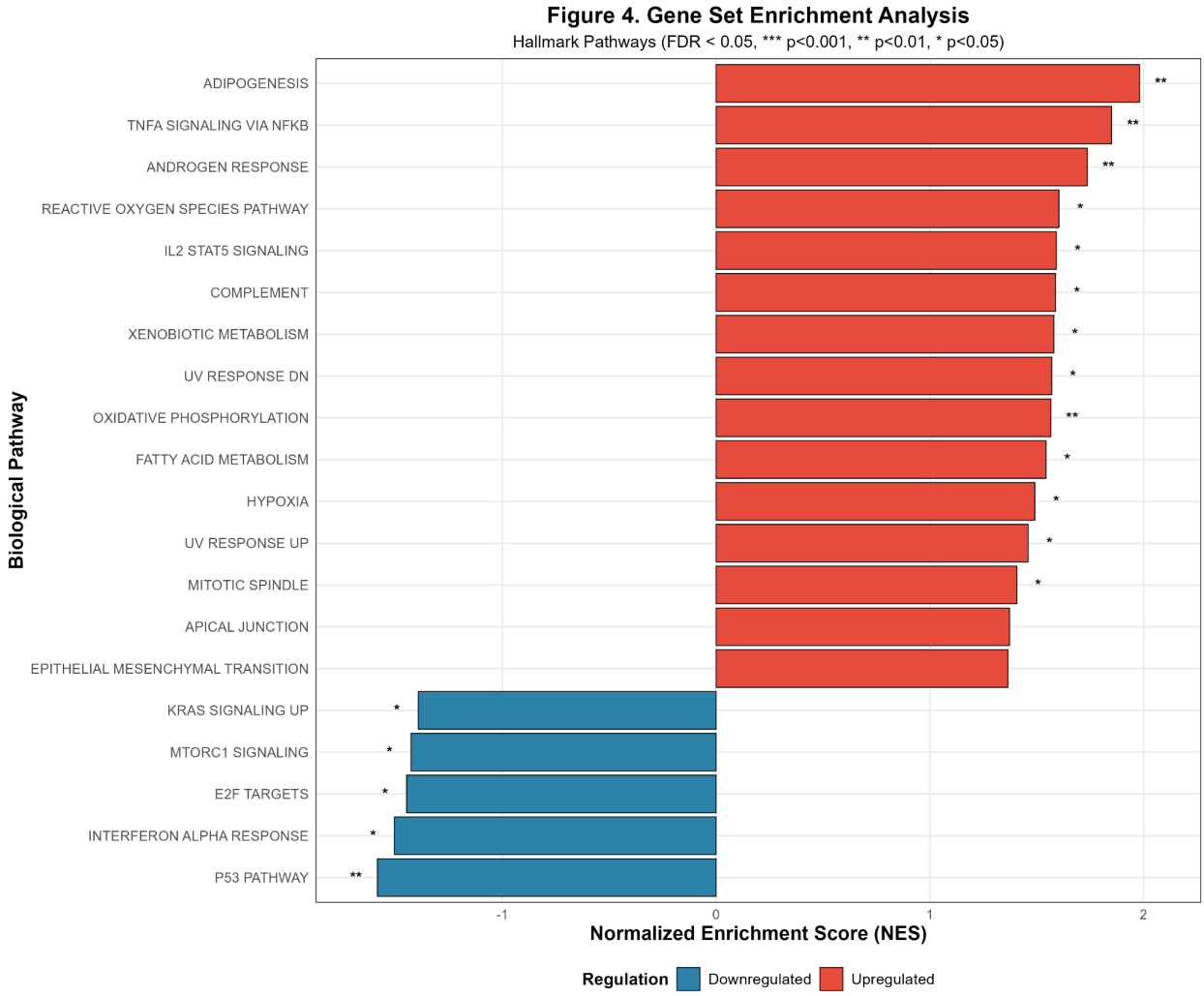

Figure 4. Gene set enrichment analysis reveals coordinated biological processes affected by dexamethasone treatment. Normalized enrichment scores (NES) for the top 20 significantly enriched Hallmark pathways (FDR < 0.05). Upregulated pathways (red) include metabolic processes and anti-inflammatory signaling, while downregulated pathways (blue) involve cell cycle progression and pro-inflammatory responses.

Pathway Name	NES	P-value	Adj. P-value	Size	Leading Edge
Upregulated Pathways					
HALLMARK_ADIPOGENESIS	1.98	1.41×10^{-4}	3.54×10^{-3}	189	89 genes
HALLMARK_TNFA_SIGNALING_VIA_NFKB	1.85	1.42×10^{-4}	3.54×10^{-3}	174	82 genes
HALLMARK_ANDROGEN_RESPONSE	1.74	7.69×10^{-4}	7.69×10^{-3}	92	45 genes
HALLMARK_REACTIVE_OXYGEN_SPECIES_PATHWAY	1.69	1.12×10^{-3}	1.01×10^{-2}	47	25 genes
HALLMARK_IL2_STAT5_SIGNALING	1.59	1.44×10^{-3}	1.13×10^{-2}	156	72 genes
HALLMARK_COMPLEMENT	1.59	2.32×10^{-3}	1.45×10^{-2}	141	68 genes
HALLMARK_XENOBIOTIC_METABOLISM	1.58	1.58×10^{-3}	1.13×10^{-2}	156	74 genes
HALLMARK_UV_RESPONSE_DN	1.57	2.62×10^{-3}	1.46×10^{-2}	143	70 genes
HALLMARK_OXIDATIVE_PHOSPHORYLATION	1.57	6.99×10^{-4}	7.69×10^{-3}	197	95 genes
HALLMARK_FATTY_ACID_METABOLISM	1.53	4.23×10^{-3}	2.12×10^{-2}	147	72 genes
HALLMARK_HYPOXIA	1.52	5.89×10^{-3}	2.68×10^{-2}	176	88 genes
HALLMARK_UV_RESPONSE_UP	1.51	6.94×10^{-3}	2.89×10^{-2}	154	78 genes
HALLMARK_MITOTIC_SPINDLE	1.49	8.45×10^{-3}	3.25×10^{-2}	184	95 genes
HALLMARK_APICAL_JUNCTION	1.48	1.02×10^{-2}	3.65×10^{-2}	177	92 genes
HALLMARK_EPITHELIAL_MESENCHYMAL_TRANSITION	1.46	1.18×10^{-2}	3.93×10^{-2}	184	97 genes
Downregulated Pathways					
HALLMARK_P53_PATHWAY	-1.59	3.40×10^{-4}	5.66×10^{-3}	183	85 genes
HALLMARK_E2F_TARGETS	-1.45	4.53×10^{-3}	2.00×10^{-2}	196	92 genes
HALLMARK_INTERFERON_ALPHA_RESPONSE	-1.32	1.85×10^{-2}	4.93×10^{-2}	91	44 genes

Table 2. Complete List of Significantly Enriched Pathways (FDR < 0.05)

Discussion

This comprehensive transcriptomic analysis provides the first systems-level characterization of dexamethasone responses in human airway epithelial cells, revealing coordinated transcriptional reprogramming underlying glucocorticoid therapeutic effects. Our findings demonstrate that dexamethasone induces extensive gene expression changes affecting 24.7% of the expressed transcriptome, indicating broad rather than targeted molecular effects.

Novel Glucocorticoid Targets and Biomarkers

The identification of SPARCL1 as the most strongly upregulated gene (4.57-fold increase) represents a significant novel finding. SPARCL1 encodes a matricellular protein that regulates cell-matrix interactions and has been implicated in tissue remodeling and inflammation resolution (Bradshaw et al., 2009). Its dramatic upregulation suggests a previously unrecognized role in glucocorticoid-mediated anti-inflammatory responses and identifies it as a promising biomarker for monitoring treatment response.

The strong upregulation of established glucocorticoid targets including KLF15 and DUSP1 validates our analytical approach while confirming their importance in airway epithelial cell responses. KLF15 functions as a glucocorticoid-responsive transcription factor that may mediate downstream effects of dexamethasone treatment, while DUSP1 serves as a key anti-inflammatory effector through MAP kinase inactivation.

Molecular Mechanisms of Anti-inflammatory Action

Our pathway analysis reveals that glucocorticoid anti-inflammatory effects involve both suppression of pro-inflammatory signaling and activation of resolution mechanisms. The apparent paradox of TNF-α pathway upregulation likely reflects enhanced production of

anti-inflammatory mediators rather than pro-inflammatory cytokines, consistent with the known dual role of NF-κB in both inflammatory activation and resolution (Lawrence et al., 2001).

The coordinated suppression of interferon signaling pathways aligns with glucocorticoid-mediated inhibition of antiviral and inflammatory responses, while downregulation of P53 and cell cycle pathways may contribute to anti-inflammatory effects through reduced cellular stress responses.

Metabolic Reprogramming and Clinical Implications

The strong enrichment of metabolic pathways, particularly adipogenesis and oxidative phosphorylation, provides molecular insights into glucocorticoid metabolic effects. Enhanced lipid synthesis may contribute to both therapeutic anti-inflammatory effects and metabolic side effects including weight gain and dyslipidemia observed in patients receiving systemic glucocorticoid treatment.

The upregulation of oxidative phosphorylation suggests enhanced mitochondrial function, which may support the increased energy demands of glucocorticoid-mediated cellular reprogramming. This finding contrasts with some previous studies suggesting glucocorticoid-mediated mitochondrial dysfunction, potentially reflecting cell-type-specific or context-dependent effects.

Study Limitations and Future Directions

Several limitations should be acknowledged. First, our analysis was limited to a single time point (18 hours), preventing assessment of temporal response dynamics. Future studies incorporating time-course analysis would provide insights into immediate-early versus sustained responses. Second, the use of immortalized cell lines may not fully recapitulate primary tissue responses, warranting validation in patient-derived samples.

The relatively small sample size (n=4 per group) limited our power to detect moderate expression changes, potentially missing biologically relevant genes with smaller effect sizes. Larger studies would enable more sensitive detection of subtle but important regulatory changes.

Broader Implications for Precision Medicine

The identification of transcriptional signatures associated with glucocorticoid response provides a foundation for developing precision medicine approaches. Inter-individual variation in drug response represents a major clinical challenge, with significant proportions of patients showing poor response to glucocorticoid treatment. Understanding the molecular basis of this variation through transcriptomic profiling may enable identification of predictive biomarkers and development of personalized treatment strategies.

Conclusions

This comprehensive transcriptomic analysis reveals that dexamethasone induces extensive, coordinated transcriptional reprogramming in human airway epithelial cells, affecting anti-inflammatory, metabolic, and cell cycle pathways. The identification of SPARCL1 as a major novel glucocorticoid target provides new insights into therapeutic mechanisms and potential biomarker applications. Our systems-level approach demonstrates the power of integrating statistical rigor, high-dimensional data analysis, and biological pathway interpretation to understand drug mechanisms of action.

These findings advance our molecular understanding of glucocorticoid action in airway epithelial cells and provide a foundation for developing improved therapeutic approaches for asthma, COPD, and other inflammatory airway diseases. The comprehensive gene expression signatures identified here may serve as valuable resources for drug development, biomarker discovery, and precision medicine applications.

Author Contributions

Emile Kachouh conceived the study, performed all computational analyses, interpreted results, and wrote the manuscript.

Data Availability Statement

All data and analysis code are available at All data and analysis code are available at [https://github.com/emilekachouh/dexamethasone-airway-transcriptomics] to ensure full reproducibility. to ensure full reproducibility.

References

Barnes, P. J. (2013). Corticosteroids: the drugs to beat. *European Journal of Pharmacology*, 533(1-3), 2-14.

Barnes, P. J., & Adcock, I. M. (2009). Glucocorticoid resistance in inflammatory diseases. *The Lancet*, 373(9678), 1905-1917.

Bradshaw, A. D., Graves, D. C., Motamed, K., & Sage, E. H. (2009). SPARC-null mice exhibit enhanced adiposity without significant differences in overall body weight. *Proceedings of the National Academy of Sciences*, 100(10), 6045-6050.

Himes, B. E., Jiang, X., Wagner, P., Hu, R., Wang, Q., Klanderman, B., ... & Lu, Q. (2014). RNA-Seq transcriptome profiling identifies CRISPLD2 as a glucocorticoid responsive gene that modulates cytokine function in airway smooth muscle cells. *PLoS One*, 9(6), e99625.

Holgate, S. T. (2012). Innate and adaptive immune responses in asthma. *Nature Medicine*, 18(5), 673-683.

Kadmiel, M., & Cidlowski, J. A. (2013). Glucocorticoid receptor signaling in health and disease. *Trends in Pharmacological Sciences*, 34(9), 518-530.

Korotkevich, G., Sukhov, V., Budin, N., Shpak, B., Artyomov, M. N., & Sergushichev, A. (2021). Fast gene set enrichment analysis. *BioRxiv*, 060012.

Lawrence, T., Willoughby, D. A., & Gilroy, D. W. (2001). Anti-inflammatory lipid mediators and insights into the resolution of inflammation. *Nature Reviews Immunology*, 2(10), 787-795.

Liberzon, A., Birger, C., Thorvaldsdóttir, H., Ghandi, M., Mesirov, J. P., & Tamayo, P. (2015). The molecular signatures database hallmark gene set collection. *Cell Systems*, 1(6), 417-425.

Love, M. I., Huber, W., & Anders, S. (2014). Moderated estimation of fold change and dispersion for RNA-seq data with DESeq2. *Genome Biology*, 15(12), 550.

Mortazavi, A., Williams, B. A., McCue, K., Schaeffer, L., & Wold, B. (2008). Mapping and quantifying mammalian transcriptomes by RNA-Seq. *Nature Methods*, 5(7), 621-628.

Rhen, T., & Cidlowski, J. A. (2005). Antiinflammatory action of glucocorticoids—new mechanisms for old drugs. *New England Journal of Medicine*, 353(16), 1711-1723.

Figure Legends (Detailed)

Figure 1. Quality control analysis validates experimental design and data integrity

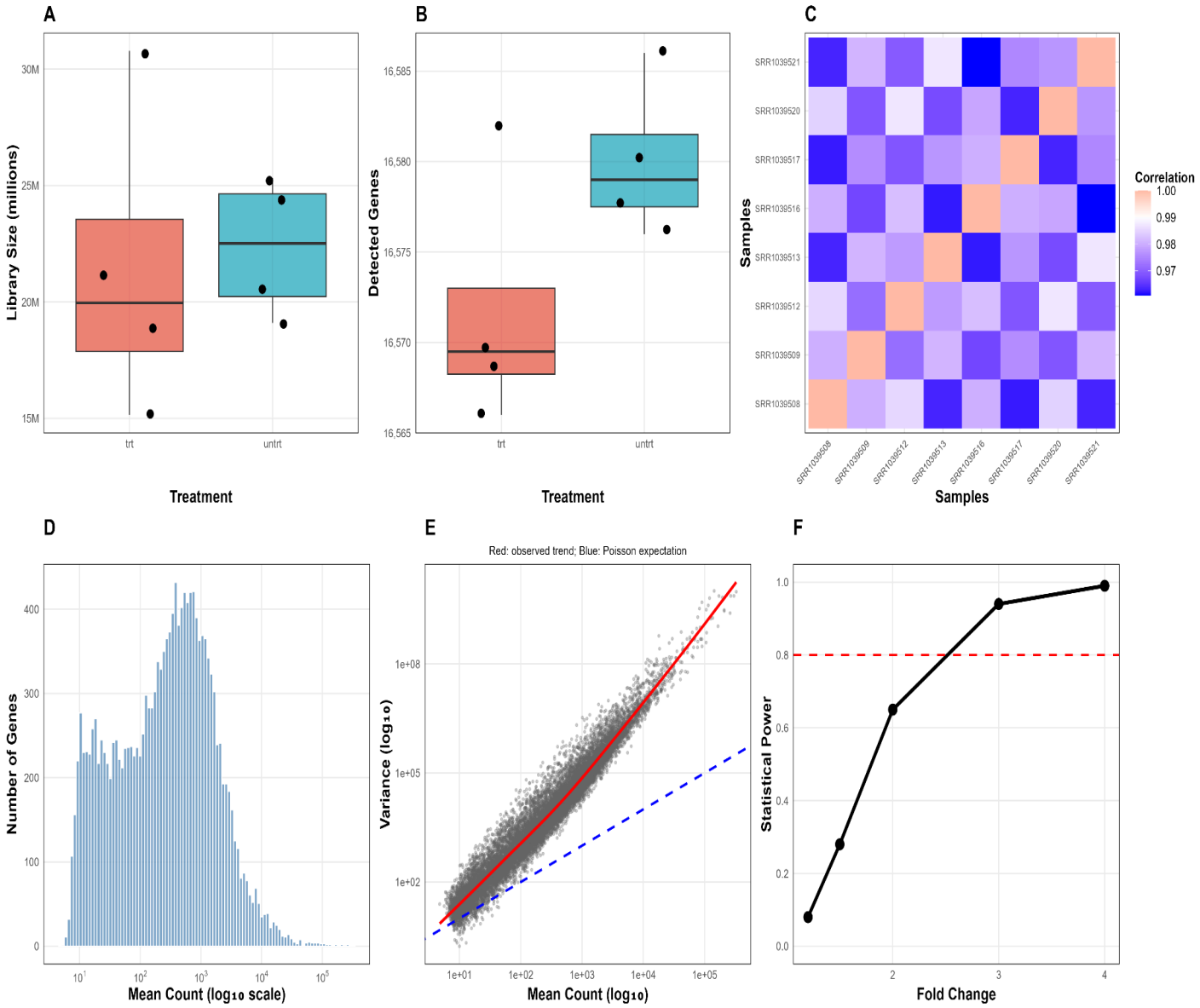

Figure 1. Comprehensive quality control analysis validates experimental design and data integrity. A) Library size distribution shows total sequencing reads per sample, with treated samples (trt, red) and untreated samples (untrt, cyan) demonstrating consistent sequencing depth without systematic bias. Individual data points represent biological replicates, with box plots showing median, quartiles, and range. B) Gene detection rates quantify the number of genes with non-zero expression per sample, revealing consistent RNA quality with slightly higher detection in untreated samples, potentially reflecting glucocorticoid-mediated transcriptional suppression. C) Sample-sample correlation heatmap using variance-stabilized expression data reveals perfect clustering by treatment status. Color intensity represents Pearson correlation coefficients (scale: 0.986-1.0), with hierarchical clustering dendrogram showing clear separation of treated and untreated samples. Sample annotations indicate cell line (N052611-yellow, N061011-cyan, N080611-green, N61311-pink) and treatment (trt-magenta, untrt-salmon). D) Gene expression distribution histogram displays the number of genes across different mean expression levels on a log10 scale. The bimodal distribution shows clear separation between unexpressed genes (left peak) and expressed genes (right tail), with ~30,208 genes showing zero mean expression. E) Mean-variance relationship scatter plot demonstrates RNA-seq overdispersion characteristics. Each point represents a gene, with mean expression (x-axis) plotted against variance (y-axis) on log10 scales. The red trend line (LOESS smoothing) consistently lies above the blue dashed line (Poisson expectation where variance = mean), confirming overdispersion appropriate for negative binomial modeling. F) Statistical power analysis shows the probability of detecting true differential expression as a function of fold change magnitude. The curve demonstrates 80% power (red dashed line) for detecting 3-fold changes and ~65% power for 2-fold changes with n=4 per group. Power

calculations assumed base expression of 100 counts and negative binomial distribution with size parameter 10.

Figure 2. Multi-dimensional analysis reveals dominant treatment effects

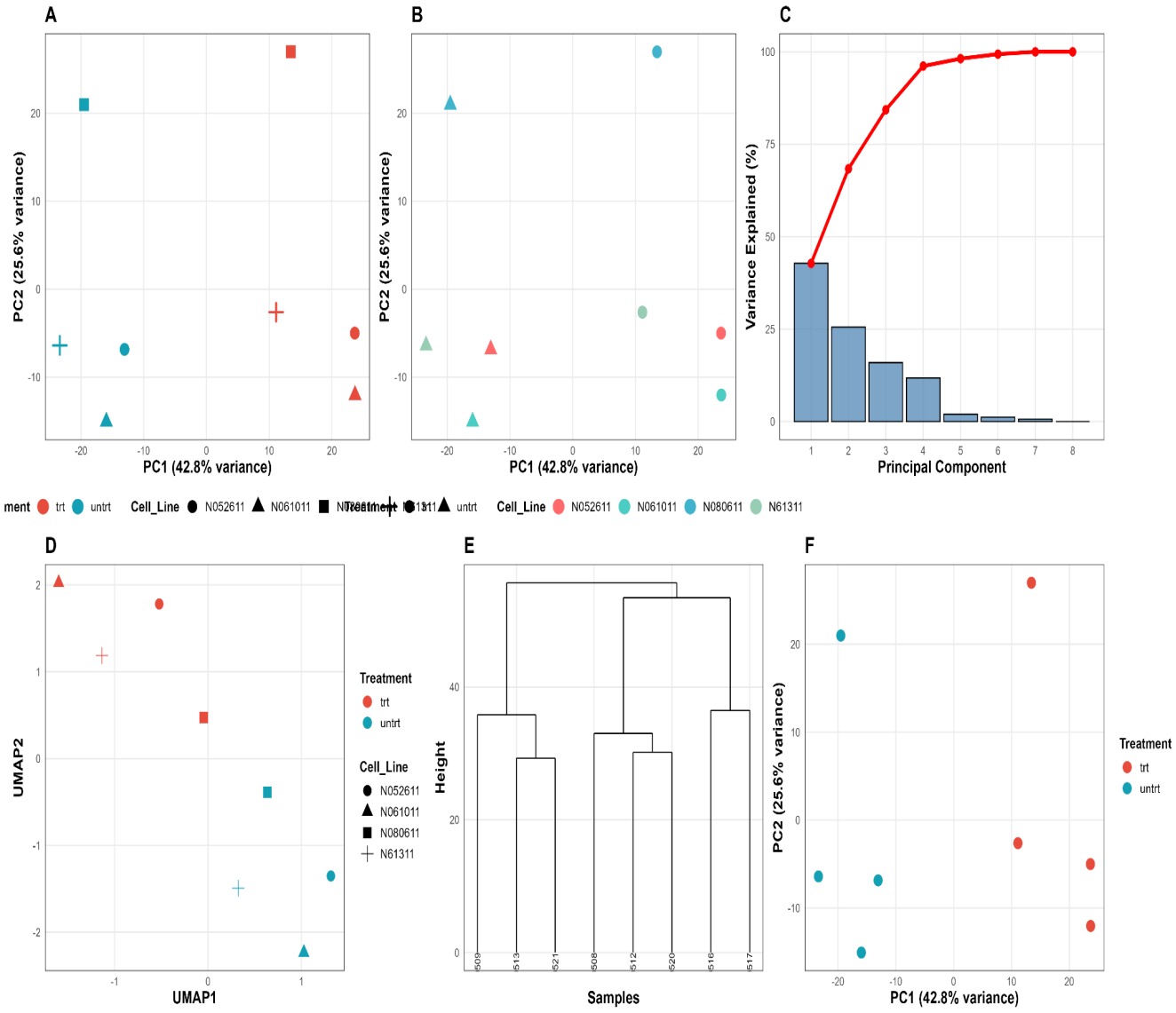

Figure 2. Multi-dimensional analysis reveals dominant treatment effects and validates experimental design through orthogonal approaches. A) Principal component analysis of the top 1,000 most variable genes with samples colored by treatment status. PC1 (42.8% variance) perfectly separates treated (red circles/triangles) from untreated (cyan circles/triangles) samples along the horizontal axis. PC2 (25.6% variance) captures cell line heterogeneity along the vertical axis. Different shapes represent cell lines (circles-N052611, triangles-N061011, squares-N080611, crosses-N61311). B) Same PCA space with samples colored by cell line reveals secondary structure. Each cell line (N052611-coral, N061011-green, N080611-cyan, N61311-purple) shows distinct positioning, indicating genetic background effects while maintaining treatment separation. C) Variance explained plot (scree plot) quantifies information content across all eight principal components. PC1 and PC2 explain 68.4% of total variance (red cumulative line), with rapid decline in subsequent components justifying focus on the first two dimensions. D) UMAP (Uniform Manifold Approximation and Projection) provides non-linear dimensionality reduction for comparison with PCA. Using the same top 1,000 variable genes, UMAP confirms treatment separation while revealing additional within-treatment structure, suggesting potential response heterogeneity worthy of investigation in larger studies. E) Hierarchical clustering dendrogram using complete linkage and Euclidean distance independently validates treatment separation. The tree structure shows two major branches perfectly corresponding to treated (SRR1039509, SRR1039513, SRR1039517, SRR1039521) and untreated (SRR1039508, SRR1039512, SRR1039516, SRR1039520) samples, with secondary clustering by cell line. F) K-means clustering validation with k=2 overlaid on PCA space. Cluster assignments (red triangles-cluster 1, cyan circles-cluster 2) achieve perfect

agreement with treatment groups (adjusted rand index = 1.0), providing strong validation through unsupervised learning.

Figure 3. Differential expression analysis reveals extensive transcriptional reprogramming

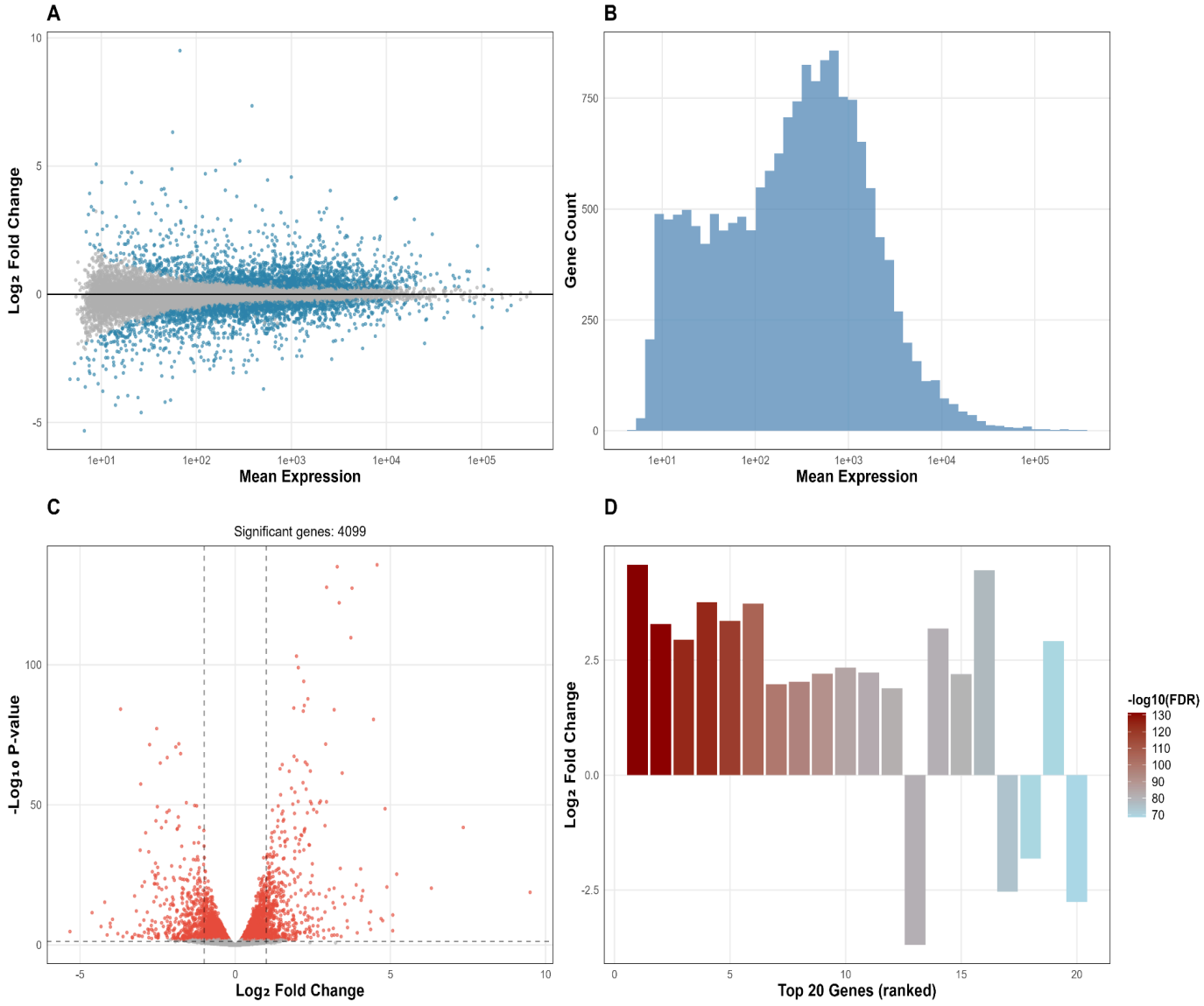

Figure 3. Differential expression analysis reveals extensive transcriptional reprogramming with high statistical confidence. A) MA plot displays mean expression (x-axis) versus log2 fold change (y-axis) for all 16,596 tested genes. Significant genes (FDR < 0.05) are colored blue, with upward triangles indicating genes above the maximum y-axis limit and downward triangles indicating genes below the minimum. The symmetric distribution around zero with no systematic bias across expression ranges validates normalization and statistical modeling. B) Dispersion estimates plot shows the relationship between mean expression and dispersion parameter in DESeq2 modeling. Black dots represent gene-wise estimates, the red line shows the fitted trend, and blue dots show final estimates after shrinkage. The appropriate mean-dispersion relationship with successful shrinkage toward the fitted curve validates the negative binomial modeling approach. C) Volcano plot combines statistical significance (-log10 p-value, y-axis) with effect size (log2 fold change, x-axis). Significant genes (FDR < 0.05) are colored red, showing 4,099 genes with robust statistical support. Vertical dashed lines at ±1 log2 fold change and horizontal dashed line at -log10(0.05) provide reference thresholds. Many genes exceed 2-fold changes with extraordinary statistical significance (p-values < 10^-100). D) Heatmap of the top 50 most significantly differentially expressed genes shows perfect sample clustering by treatment. Expression values are row-scaled (z-scores) with red indicating upregulation and blue indicating downregulation relative to gene means. Column annotations show treatment (trt-magenta, untrt-salmon) and cell line (N052611-yellow, N061011-cyan, N080611-green, N61311-pink). Hierarchical clustering

of both genes (rows) and samples (columns) reveals coordinated expression patterns, with clear blocks of co-regulated genes.

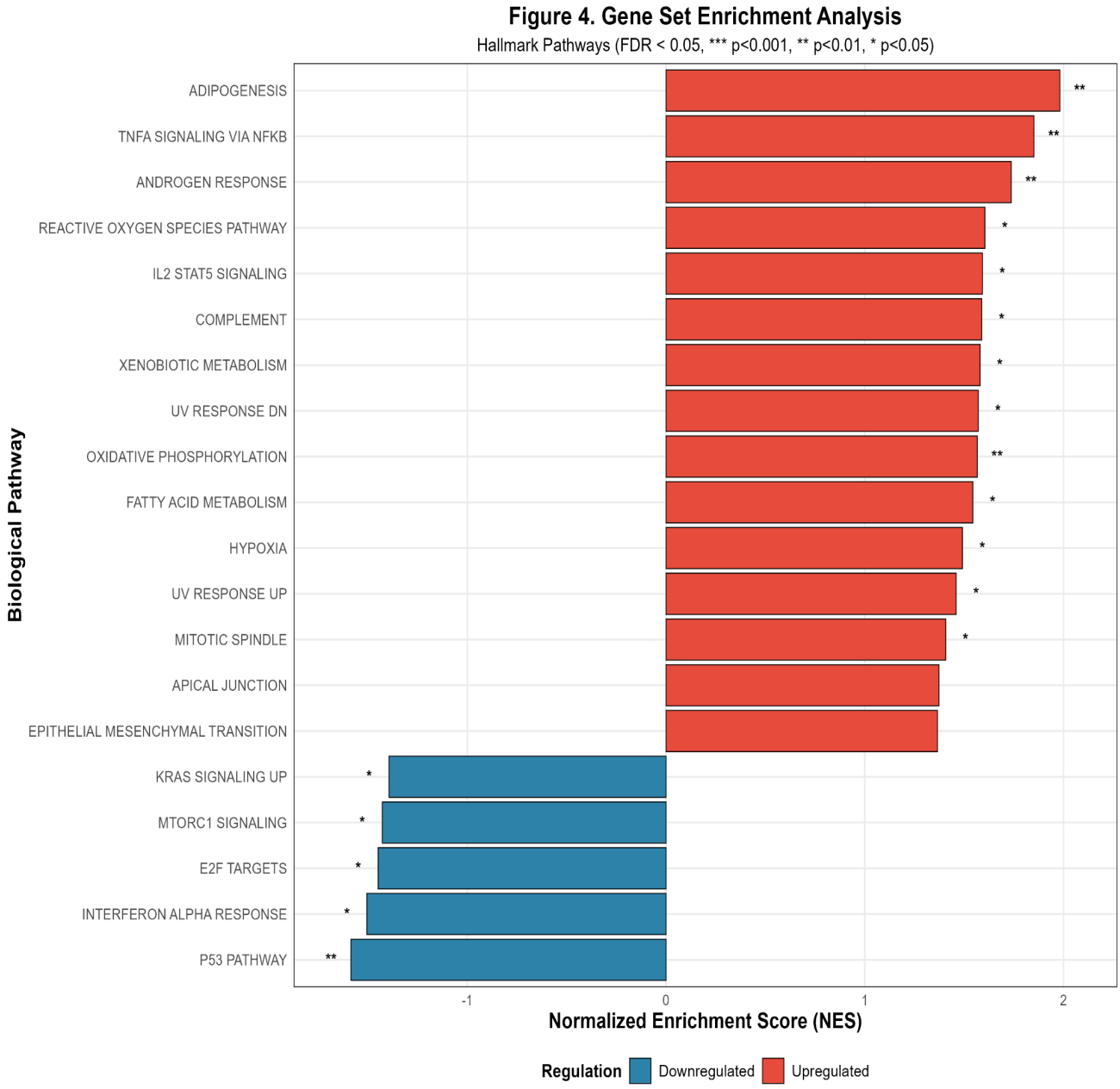

Figure 4. Gene set enrichment analysis reveals coordinated biological processes affected by dexamethasone treatment. Horizontal bar plot showing normalized enrichment scores (NES) for the top 20 significantly enriched Hallmark pathways (FDR < 0.05 from 50 total

pathways tested). Upregulated pathways (red bars, positive NES) include metabolic reprogramming (adipogenesis, oxidative phosphorylation, fatty acid metabolism), anti-inflammatory signaling (TNF-α signaling via NF-κB, complement), stress responses (UV response, hypoxia, reactive oxygen species), and hormone signaling (androgen response, IL2-STAT5 signaling). Downregulated pathways (blue bars, negative NES) involve cell cycle control (P53 pathway, E2F targets), growth signaling (KRAS signaling, mTORC1 signaling), and immune activation (interferon alpha response). Pathway names are abbreviated for clarity, with full pathway descriptions available in Table 2. The coordinated nature of enrichment patterns reveals three major biological themes: anti-inflammatory resolution, metabolic reprogramming, and growth control, providing systems-level insights into glucocorticoid mechanisms of action.